Simulation of Dose Estimations from Solar Protons: A PMMA-Bi$_2$O$_3$ Shielding Model for Space Exploration

L. Sajo-Bohus[1*] (ID)**, J.A. López[2] and M. Castro-Colin[3]**

[1]*University Simon Bolivar, Baruta 89000, Caracas, Venezuela, YV-1080A*

[2]*Department of Physics, University of Texas El Paso, TX, USA*

[3]*Bruker AXS GmbH, Karlsruhe, Germany*

[*]sajobohus@gmail.com (Corresponding Author)

ARTICLE INFORMATION

ABSTRACT

Adverse effects of long-term exposure to galactic cosmic radiation (GCR) pose a non negligible obstacle for future space exploration programs; the high-LET-particle-rich environment has an adverse effect on human health. Concomitant to GCR we have as well solar particle radiation. Long term space exploration will rely on adequate and highly efficient shielding materials that will reduce exposure of both biosystems and electronic equipment to GCR and solar particles. The shield must attenuate efficiently heavy GCR ions, by breaking them up into less-damaging fragments and secondary radiation: biologically damaging energetic neutrons and highly charged and energetic HZE- particles. An approach to this problem is the development of shielding compounds. Shielding materials should address the conditions of different aspects of a given mission, e.g. time duration and travel path. The Monte Carlo method (GEANT4) is here employed to estimate the effects of a shielding material based on the recently developed Bi$_2$O$_3$-based compound (Cao et al, 2020). In the present study GEANT4 code is used to make estimations of attenuation of solar protons. The objective is to provide some insight about the effect of the new composite shield that has an intrinsic capability for dose reduction.

1. Introduction

This year 2020, there have been already at least five missions to Mars which are scientifically very promising. As an example, the rover Curiosity, launched back in 2011 has recently been the source of multiple documented results [3, 5]. Clearly these missions and others are preparing the ground for future manned explorations. However, it has been clear to scientist and engineers alike [9], that radiation will be a concern as missions have a long-time duration, sufficient to observe adverse health effects.

The two main radiation sources of concern are galactic cosmic rays (GCR) and solar particle events (SPE). Both types of sources are mostly composed by protons [8, 11]. Supernova remnants are considered to be the most plausible candidates of GCR [8] while solar particles are thought to be produced by the sudden release of magnetic energy during solar eruptions [6].

In this study we are concerned with proton irradiation as a neutron precursor. Neutrons are highly penetrating particles that scatter elastically, inelastically, can be captured, and cause spallation. The study of Palfalvi et al. [7], which used solid state nuclear track detectors placed inside the International Space Station, registered about 20% neutron particle content. Thus it became a sizable contributor to radiation dose.

Neutrons are neither part of the GCR nor the SPE. They are however spalled by both. Wilson et al. [10] have used neutrons generated by GCR spallation to measure the lifetime of the neutron—about 760s.

In this paper we focus on SPE, specifically solar protons. Subsequently, in a different study, we will apply the same approach to the proton spectral component of GCR.

The shielding material used in the model here studied was experimentally studied by Cao et al. [2]. It was developed originally as a gamma shielding material, but its percentage content of poly (methyl methacrylate) (PMMA) makes it also a candidate as a neutron shield. Similar Bi$_2$O$_3$-based materials have been investigated as neutron and gamma shielding materials [4].

2. Simulation description and methods

Our approach consisted on selecting a spectral distribution of solar protons. We use the fluence curve vs. energy

[MeV] presented by Xapsos et al. [11]. The experimental points from 4 August event [11] were digitized and used as precursor for Monte Carlo simulations with Geant4 [1].

To facilitate analysis, fluence values were not simulated using the number of events shown, which range from 10^7 to 10^{10} 1/cm², Figure 1. Fluence values were scaled down to 100 events at the neutron energy of 150 MeV and up to about 77×10^3 events at 10 MeV.

The model consists of three layers: shield, gap, and muscular tissue. Density values for each material were taken directly from the database of Geant4. They are NIST compounds as well as from the HEP and materials databases. In the present case we have 4.577 g/cm³, 1×10^{-25} g/cm³, and 1.050 g/cm³, for the shield, gap, and muscular tissue, respectively.

Shielding material is a composite of PMMA, density = 1.180 g/cm³, with 44 wt.% Bi_2O_3, density = 8.9 g/cm³. For the purposes of the simulation the material is homogeneous.

The simulations follow the next protocol:

1. A scaled-down proton fluence value is selected.
2. From the histograms generated by Geant4 all neutrons that arise as secondary particles are selected as well as their depth of creation and kinetic energies. Thus from each fluence value we have a collection of kinetic energies and creation depths that will be used during a subsequent step.
3. Estimation of the reduced shield thickness, t. We use the following formulation.

$$t = T - d,$$

where:

    t = reduced shield thickness,
    T = nominal shield thickness, 100 mm,
    $d = \Sigma \, (n(E_i) \, \delta(E_i)) / \Sigma \, n(E_i)$,
    d = weighed depth of neutron generated as a secondary particle,
    $n(E_i)$ = number of neutrons—secondary particles—with a kinetic energy E_i,
    $\delta(E_i)$ = depth of creation of neutron—secondary particle—with kinetic energy E_i.

4. Estimation of bin size, K, and number of neutron events per bin, N. Bin sizes are estimated using Doane's formula [Doane 1976]. Bin sizes selected with this formulation are adequate for event distributions that are not normally distributed—our case.

$$K = 1 + \log_2(\eta) + \log_2(1 + |\mu_3| / s),$$

where:

    η = all observations, or in this case, all secondary particles that are neutron events.
    μ_3 = third standardized moment of skewness,

$$s = \sqrt{[6 \, (\eta - 2) \, (\eta + 1)^{-1} \, (\eta + 3)^{-1}]}$$

Once K is calculated, N is obtained:
$N = \Sigma \, n(E_i)$, if E_i is within the bin width boundaries.
Bin width boundaries are established after identifying the maximum and minimum energies and after partitioning the whole energy interval.
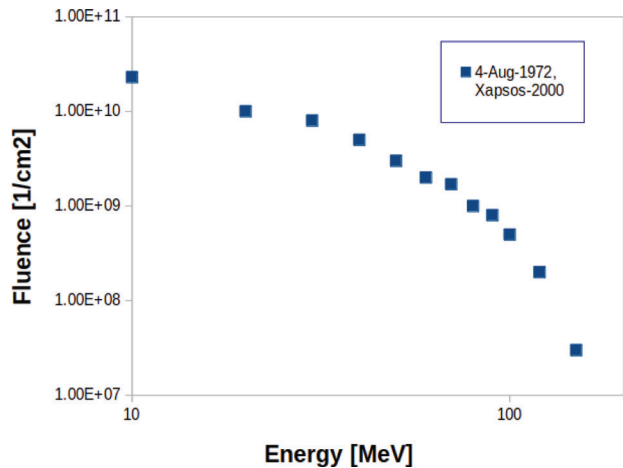
Figure 1: Solar proton fluence spectral distribution used in the simulation. The values correspond to the solar event from August 4, 1972. Digitized from Xapsos et al. [11].

5. Estimation of the energy value per bin, ε_k. This value is a simple energy average within those available in the bin ε_k. It becomes the kinetic energy of the primary particles, or neutron fluence used in the subsequent Monte Carlo set of simulations.
6. Selection of all events that deposit energy within the muscular tissue volume.
7. All particles are classified and their respective energies are added up. The types of particles—secondaries—identified were: neutron, proton, gamma, alpha, O(16), C(12), N(14), e⁻, deuteron, and alpha particles.
8. The factor used to scale down the fluence at step 1 is now used to restore the fluence value.
9. Dose values are calculated.

The process described above entailed simulating a reduced shield thickness of 67 mm for 120 MeV protons, up to 77 mm for 50 MeV.

Several models are available in Geant4 to simulate particle events. For protons we used the models: hElasticCHIPS, FTFP, and Bertini Cascade—the latter two for inelastic hadronic processes. For gamma photons: Bertini Cascade and The oFS Generator. For e⁻: G4 ElectroVD Nuclear Model. For deuterons: hElasticLHEP, Binary Light Ion Cascade, and FTFP. For alpha: hElasticLHEP, Binary Light Ion Cascade, and FTFP. For ions: BinaryLightionCascade and FTFP. For neutrons: hElasticCHIPS, FTFP, Bertini Cascade, and nRadCapture.
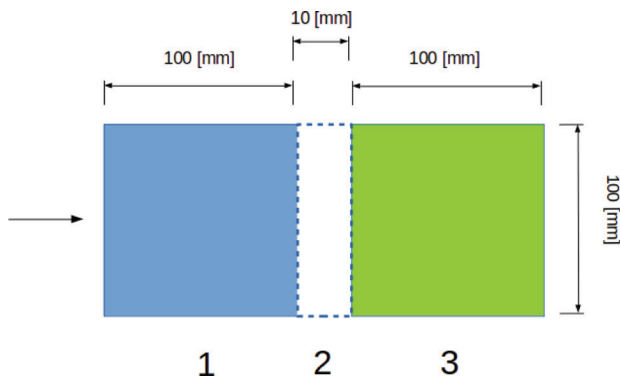
Figure 2: The geometry of the model used in the simulation consists of three layers: shield (1), gap (2), and muscular tissue (3). Densities are 4.577 g/cm^3, 1×10^{-25} g/cm^3, and 1.050 g/cm^3, respectively. The cross section has dimensions of 100×100 cm^2, and the thicknesses are as indicated: shield 100 mm, gap 10 mm, and muscular tissue 100 mm. The proton beam impinges from the left, right at the center of the shield, and has no dimensions. Kinetic energy will vary according to the values on Figure 1.

3. Results and discussion

Experience with the ISS [7] indicated that neutrons contribute near 20% to the dose. Thus the strategy here followed used protons as primaries, from which all secondary particles—neutrons—were identified as indicated in Sec. 2. With the reduced thickness values we simulated a neutron beam, corresponding to each fluence value from Figure 1.

Da Cao et al. [2] explored experimentally various wt% compositions of Bi_2O_3 and PMMA. We have only explored one composition but will study the rest of them in a subsequent study.

The process described in Sec. 2 yielded the spectral distribution of neutron kinetic energies displayed in Table 1. Those energies were estimated after binning secondary particles—neutrons—generated by proton impacts within the radiation shield. Once again, the approach was inspired by the experimental results mentioned above [7]. Neutron radiation is thus expected to be originated by protons from SPE and GCR. To be systematic, we have looked during a first approach to solar protons. Though both SPE and GCR are of concern, from our vantage point within the solar system, SPE are of greater relevance.

Neutrons will interact with the radiation shield and be the precursors of additional particles: neutron, proton, gamma, alpha, O(16), C(12), N(14), e$^-$, deuteron, and alpha particles.

Histograms from Geant4 yielded information about the type of particle and the energy that it deposited within each of the layers. Spectral distribution of neutrons is summarized, Table 1.

Table 1: The process described in Sec. 2 helped us to generate a neutron spectral distribution. These energies are the primary particles in simulations with the corresponding reduced shield thickness.

Proton energy [MeV]	Reduced shield thickness [mm]	Kinetic energy of neutrons (secondary particles) [MeV]
50	77	1.02340
60	75	1.05775
		3.74750
		19.60000
70	74	1.04000
		5.04500
		9.34000
		34.50000
80	71	1.45100
		20.30000
		41.20000
90	70	1.49600
		7.24500
		15.40000
		43.20000
100	69	1.24900
		5.30300
		7.89000
		10.9670
		23.2000
120	67	1.64400
		5.48100
		10.30700
		29.30000
		42.65000
		61.75000

Protons did not deposit energy directly in the muscular tissue. However, secondary particles did deposit energy. Therefore secondary particles, neutrons, were selected from the histograms as describe in Sec. 1. Figure 3 shows an example of simulated neutron tracks of 1 MeV, that resulted from protons of 50 MeV. The simulation corresponds to the first row of Table 1. As it is expected, the reduced shield thickness is larger for smaller proton energies, conversely the reduced shield thickness is thinner for larger proton kinetic energies.

Tables 2 and 3 summarize the dose deposited by each type of secondary particle after simulating neutron irradiation with the energies in Table 1.
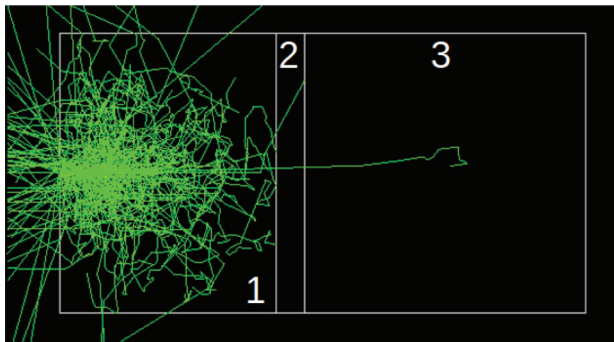
Figure 3: Example of neutron tracks of 1 MeV kinetic energy, created by a proton beam of 50 MeV. All three layers of the model can be observed: shielding (1), rarefied medium or gap (2), and muscular tissue (3).
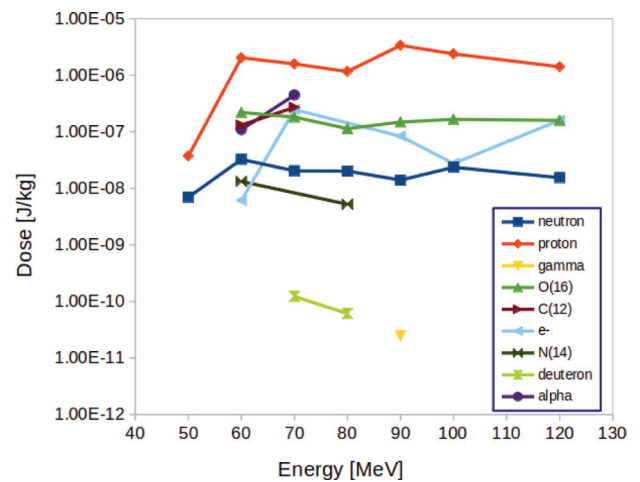
Figure 4: The dose values from Tables 2 and 3 are represented in this figure. Gamma photons have the lowest dose contributions while protons have the highest. Note that these are particles generated by neutrons and not directly by solar protons.

Table 2: Dose values were calculated for each type of particle identified as a secondary which deposited energy within the muscular tissue layer. Additional particles and their respective dose values are in the complementary Table 3.

Proton energy [MeV]	Dose [J/kg]				
	Neutron	**Proton**	**Gamma**	**O(16)**	**C(12)**
50	6.982E-09	3.739E-08			
60	3.253E-08	2.039E-06		2.200E-07	1.312E-07
70	2.036E-08	1.585E-06		1.817E-07	2.711E-07
80	2.020E-08	1.166E-06		1.136E-07	
90	1.399E-08	3.373E-06	2.458E-11	1.485E-07	
100	2.356E-08	2.386E-06		1.659E-07	
120	1.543E-08	1.412E-06		1.590E-07	

Table 3: Dose values were calculated for each type of particle identified as a secondary which deposited energy within the muscular tissue layer. This table is complementary to Table 2.

Proton energy [MeV]	Dose [J/kg]			
	e⁻	**N(14)**	**Deuteron**	**Alpha**
50				
60	6.080E-09	1.323E-08		1.094E-07
70	2.464E-07		1.222E-10	4.473E-07
80		5.219E-09	6.089E-11	
90	8.348E-08			
100	2.742E-08			
120	1.599E-07			

Dose values from Tables 2 and 3 are plotted, Figure 4, to facilitate visualization of average dose trends. Lines are only used as an aid to the eye, to identify better particles of the same type. It would be expected to have continuous lines for all types of particles such that they span the whole energy range between 50 MeV and 120 MeV.

Protons (secondaries) have the largest average dose. Of course the dose equivalent values have to be calculated after considering the respective Q factors. As we know, ions have larger Q factors and considered biologically more harmful.

Summary

We have studied the efficiency of $PMMABi_2O_3$ to mitigate solar proton radiation, as primary particles and their secondary particles. With a simple three-layer model, we simulated energy deposition in a muscular tissue layer using GEANT4. Two main aspects are highlighted in this study. On the one hand, it is a simple model that contains a minimum of variables to simulate shielding effectiveness of $PMMA-Bi_2O_3$. On the other hand it presents a procedure that could be used with small computers that may not have the capacity to process large fluence values.

The lack of particles throughout the whole range of proton kinetic energies and thus of energy deposited by some of the particles identified, Figure 4, may be the result of the method employed. This event can be verified by increasing the number of particles simulated, thus reducing the scaling factor. Gamma photons were barely detected, as shown in Figure 4, which may be expected on a gamma shield as is the case of $PMMA-Bi_2O_3$.

Most importantly, the study gives some values that should be verified experimentally. However, validation of the model can also be accomplished using an aluminum shield with thickness values found in the ISS. In that case dose values could be readily matched to the experimental results of Palfalvi et al. [7].

Acknowledgments

References

[1] S. Agostinelli, J. Allison, K. Amako, J. Apostolakis, H. Araujo, P. Arcel, M. Asai, D. Axen, S. Banerjee, G. Barrand, F. Behner, L. Bellagamba, J. Boudreau, L. Broglia, A. Brunengo, H. Burkhardt, S. Chauvie, J. Chuma, R. Chytracek, G. Cooperman and D. Zschiesche, Nuclear Instruments and Methods in Physics Research Section A: Accelerators, Spectrometers, Detectors and Associated Equipment **506**, 250 (2003). https://doi.org/10.1016/S0168-9002(03)01368-8

[2] D. Cao, G. Yang, M. Bourham and D. Moneghan, Nuclear Engineering and Technology **52**, 2613 (2020). https://doi.org/10.1016/j.net.2020.04.026

[3] R. Francis, T. Estlin, G. Doran, S. Johnstone, D. Gaines, V. Verma, M. Burl, J. Frydenvang, S. Montaño, R.C. Wiens, S. Schaffer, O. Gasnault, L. DeFlores, D. Blaney and B. Bornstein, Science Robotics **2**, eaan4582 (2017). https://doi.org/10.1126/scirobotics.aan4582

[4] S.A.M. Issa, M. Ahmad, H.O. Tekin, Y.B. Sadeek and M.A. Sayyed, Results in Physics **13**, 102165 (2019). https://doi.org/10.1016/j.rinp.2019.102165

[5] K.W. Lewis, S. Peters, K. Gonter, S. Morrison, N. Schmerr, A.R. Vasavada and T. Gabriel, Science **363**, 535 (2019). https://doi.org/10.1126/science.aat0738

[6] L.I. Miroshnichenko, Journal of Space Weather and Space Climate **8**, A52 (2018). https://doi.org/10.1051/swsc/2018042

[7] J.K. Palfalvi, Y. Akatov, J. Szabo, L. Sajo-Bohus and I. Eordogh, Radiation Protection Dosimetry **120**, 427 (2006). https://doi.org/10.1093/rpd/nci673

[8] S. Thoudam, J.P. Rachen, A. van Vliet, A. Achterberg, S. Buitink, H. Falcke and J.R. Hoerandel, Astronomy and Astrophysics **595**, A33 (2016). https://doi.org/10.1051/0004-6361/201628894

[9] J.W. Wilson, F.A. Cucinotta, J.L. Shinn, M.-H. Kim and F.F. Badavi, Preliminary Considerations edited by J.W. Wilson, J. Miller, A. Konradi and F. A. Cucinotta, *Shielding Strategies for Human Space Exploration,* NASA Conference Publication 3360. Ch. 1, pp. 3-15 (1997).

[10] J.T. Wilson, D.J. Lawrence, P.N. Peplowski, V.R. Ecke and J.A. Kegerreis, Physical Review Research **2**, 023316 (2020). https://doi.org/10.1103/PhysRevResearch.2.023316

[11] M.A. Xapsos, J.L. Barth, E.G. Stassinopoulos, S.R. Messnger, R.J. Walters, G.P. Summers, and E.A. Burke. IEEE Transactions on Nuclear Science **47**, 2218 (2000). https://doi.org/10.1109/23.903756

Journal of Nuclear Physics, Material Sciences, Radiation and Applications